Superconducting Tunnel Junctions

Shantanu Jha and Chris West
(Dated: February 21st, 2019)

The superconducting gap in energy states is a characteristic property of a metal and described by the Bardeen-Cooper-Schrieffer theory. Here, we measure the gap of lead and aluminum, finding values of $\Delta_{Pb} = 1.18 \pm .02$meV at around 4.2K and $\Delta_{Pb} = 1.36 \pm .01$meV, $\Delta_{Al} = .06 \pm .01$meV at around 1.4K. Through demonstrating reasonable uncertainty estimates in χ^2_ν fit parameters, χ^2_ν values, and residuals, we are confident in our results.

I. INTRODUCTION

When cooled to extreme temperatures, some metals exhibit superconducting behavior that creates a gap in the available energy states of their electrons. In practice, this means that when configured in a junction, a finite voltage difference is required between two metals for a current flow to be observed. At the critical temperature (when superconducting properties begin to manifest) of a metal x, the half-width of this superconducting energy gap is denoted Δ_x.

In this experiment, we measure the superconducting gap of two metals, lead and aluminum. To this end, we collect three sets of data, each at different temperatures. A thorough χ^2 minimization process will fit our data to relevant theory, and find our experimental values for the superconducting gaps, Δ_{Pb} and Δ_{Al}.

In order to isolate the effects of the superconducting gap of each metal, we aim to examine three junction regimes with respect to the state (normal / superconducting) of the two metals; normal - insulator - normal (NIN), superconducting - insulator - normal (SIN), and superconducting - insulator - superconducting (SIS).

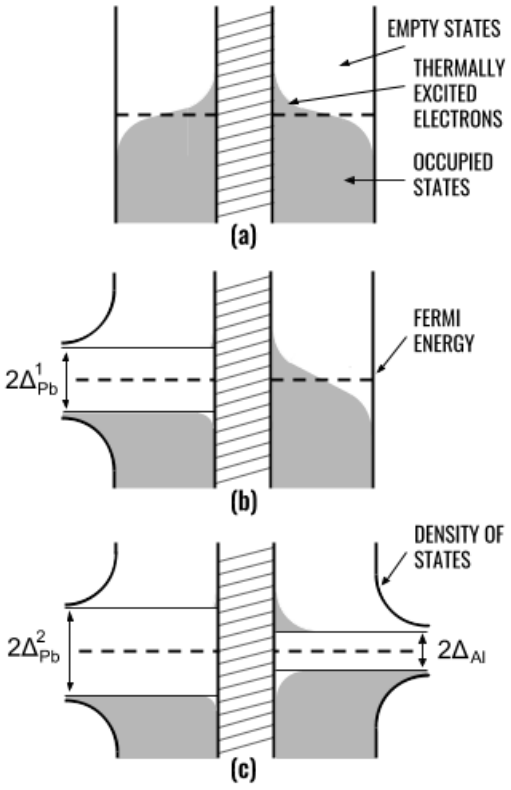

Figure I.1. Possible energy states at zero voltage for the (a) NIN, (b) SIN, and (c) SIS regimes. Lead is on the left and aluminum is on the right, separated by an insulating barrier. Δ^1_{Pb} is the characteristic gap of lead, while Δ^2_{Pb} is the slightly larger gap resultant from a decrease in temperature between the SIN and SIS regimes. Adapted from [3].

A. NIN

When both metals are at room temperature (well above their critical temperatures), we have the NIN regime. Fig. I.1 (a) shows the possible energy states when zero voltage is applied. There is tunnelling occurring, but electrons tunneling from lead to aluminum cancel those tunneling from aluminum to lead, resulting in zero current. When a voltage is applied, the baseline voltage difference between the metals changes and results in, for example, electrons on the left being able to tunnel to the right with much higher probability than in the other direction - and thus, a current flow. For the NIN regime, the expected $I(V)$ equation is

$$I_{NIN} = \frac{V}{R_o} \tag{I.1}$$

where

$$R_o = \frac{1}{eA|\mathcal{T}|^2 N_{Ln}(0) N_{Rn}(0)} \ . \tag{I.2}$$

$|\mathcal{T}^2|$ is the tunneling probability and A is a proportionality constant related to the geometry of the junction. N_{Ln} and N_{Rn} are the density of states of the left (L) and right (R) metals at normal (n) conditions (temperature-wise), and are evaluated here at energy $E = 0$. Since Eq. I.2 is a temperature-independent constant, Eq. I.1 is linear.

B. SIN

When the temperature of the apparatus is cooled below 7.2 K (the critical temperature of lead), we enter the SIN regime. Fig. I.1 (b) shows the possible energy states

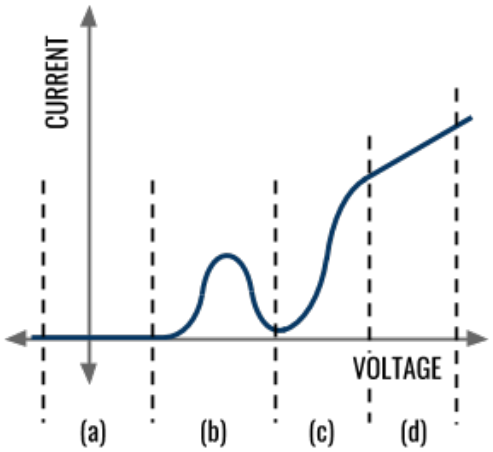

Figure I.2. A graph of the theory prediction for the $I(V)$ curve of the SIS regime at nonzero temperature. [1]

when zero voltage is applied. The superconducting gap creates a band of energy levels that no electrons may occupy. Thus, at zero voltage there is no tunneling occurring. After a small increase in voltage, the picture won't have changed much, and still no current will flow. Finally, after there is enough of a voltage difference for the normal metal (aluminum, in this case) to have electrons at energy levels equal to the energy levels of the holes of lead, tunneling will begin and current will flow. Graphically, we expect a $I(V)$ curve to be constant at zero until $V = \Delta_{Pb}/e$, at which point the current will spike up to the underlying linear value, as shown in Fig. I.2 (c) and (d). The expected $I(V)$ equation is

$$I_{SIN} = \frac{1}{eR_o}\int_{-\infty}^{+\infty} \frac{N_{Ls}(E)}{N_{Ln}(0)}[f(E) - f(E+eV)]dE \quad \text{(I.3)}$$

where N_{Ls} is the density of states of the left (L) metal (in the SIN case; lead) at superconducting conditions.

C. SIS

Finally, the system below 1.2 K (the critical temperature of aluminum[1]) is described by the SIS regime. Similar to the SIN regime, tunneling cannot occur at zero voltage due to the gaps in possible energy states for both metals (as shown in Fig. I.1 (c)). Theory predicts the $I(V)$ curve in Fig. I.2. Current does not start to flow until V gets close to $(\Delta_{Pb} - \Delta_{Al})/e$, which is when the electrons that have "smeared" above the gap of aluminum have available spots in lead that they can tunnel to. Further increase, though, causes a decrease in voltage, as any "smeared" aluminum electrons are now at higher energy levels than the available states in lead. Finally, at $V = (\Delta_{Pb} + \Delta_{Al})/e$, the gaps of the two metals are no longer overlapping, and we see the same jump in current as in the SIN regime. The expected $I(V)$ equation is

$$I_{SIS} = \frac{1}{eR_o}\int_{-\infty}^{+\infty} \frac{N_{Ls}(E)}{N_{Ln}(0)}\frac{N_{Rs}(E+ev)}{N_{Rn}(0)} [f(E) - f(E+eV)]dE \ . \quad \text{(I.4)}$$

[1] We were not working with pure aluminum, so the critical temperature is higher than $1.2K$. Effectively, this only means that the chamber may be pumped to a slightly higher pressure than if we had pure lead.

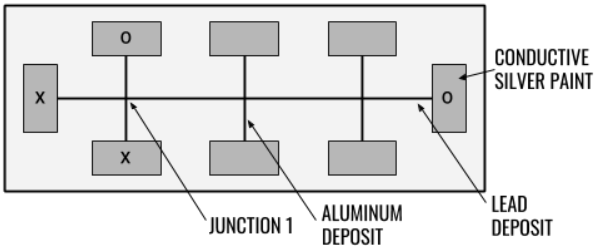

Figure II.1. A diagram of a slide. The x's indicate where current is supplied and the o's indicate where voltage is measured for Junction 1.

II. EXPERIMENTAL PROCEDURE

A. Preparation

In order to minimize contamination of the junctions, we prepared six slides - each with three junctions - using thermal evaporation. Fig. II.1 shows a diagram of a single slide. The lead layer was 4.08 kÅ thick and the aluminum layer was 1.06 kÅ thick. The slides were oxidized for approximately 6 minutes between deposition of the aluminum and the lead.

Of the six slides, a single one was chosen by roughly measuring the voltages between several contacts on each slide. We chose the slide that had the most consistent voltage differentials between symmetric contacts as described in V B. The resistances of the three junctions on this slide were tested again before data collection to ensure that they had not degraded in the days between deposition and data collection.

B. Data Collection

Since the resistances of the junctions are all small, it is easier to vary current and measure voltage than vice versa. The computer will generate a voltage that will be converted to a predictable current at the large internal resistor R_v. Then the voltage across the junction is measured with a four-point probe to reduce voltage lost across the lead and aluminum wires. The upshot is that

our data collection actually results in a $V(I)$ curve. Under normal conditions $I(V)$ is a bijective function, and thus can be inverted. However, for the SIS regime, we expect the behavior shown in Fig. I.2, which is notably not a function when the axis are flipped. This will give rise to hysteresis. Since we will be sweeping voltage in both the positive and negative directions, the domain of voltages that we aren't able to collect current data for will be minimal.

For the NIN regime, the chosen slide was loaded in the apparatus (depicted in Fig. II.2) and measurements of the three junctions were taken. For each junction, input voltage from the DAQ was varied from $-5\,\mathrm{V}$ to $5\,\mathrm{V}$, which was then converted to a known current by the internal resistor. Voltage was varied in steps of $0.02\,\mathrm{V}$ in both the negative and positive directions. The sampling rate was $10,000$ samples/sec and we collected samples for .01 seconds at each voltage. The frequency filter was set to $1000\,\mathrm{Hz}$ and the gain was set to 100. The internal resistor was set to $R_v = 10\,000\,\Omega$. These settings were not changed for the other regimes unless noted. All three junctions displayed a linear $I(V)$ curve. Given the consistency of the measured R_o values through all three of our junctions, as displayed in Table III.1, and their magnitude on the order of $10^1\Omega$, we felt comfortable continuing to the next regimes with this slide.

To get to the SIN regime, the liquid nitrogen and liquid helium were poured into the apparatus. The first junction was destroyed during the temperature change, but the second and third remained functioning well. The gain was increased to 500 and the internal resistor was switched to $100\,000\,\Omega$. For each junction, the voltage was varied from $-5\,\mathrm{V}$ to $5\,\mathrm{V}$ in a step size of $0.02\,\mathrm{V}$ in both the negative and positive directions. The expected zero current behavior was observed for small voltages. The data from both the positive and negative sweeps of junction 2 in the SIN regime are plotted together in Fig. III.5.

Finally, to get to the SIS regime, the pressure in the apparatus was decreased with a roughing pump [2]. The pressure in the innermost chamber was monitored, and we began collecting data at $1.684\,\mathrm{Torr}$. The second and third junctions functioned well after the temperature change was complete. The gain stayed at 500 and the internal resistor at $100\,000\,\Omega$. For each junction voltage was varied from $-1\,\mathrm{V}$ to $1\,\mathrm{V}$ in a step size of $0.004\,\mathrm{V}$ in both the negative and positive directions. The smaller step size was selected in order to get greater clarity of the hysteresis effect. The smaller voltage range was selected to minimize the run time of the collection. The expected hysteresis effect was observed in both cases. The data from both the positive and negative sweeps of junction 2 in the SIS are plotted together in Fig. III.6.

[2] A decrease in pressure causes a decrease in boiling point, which allows us to manipulate the temperature of the liquid helium.

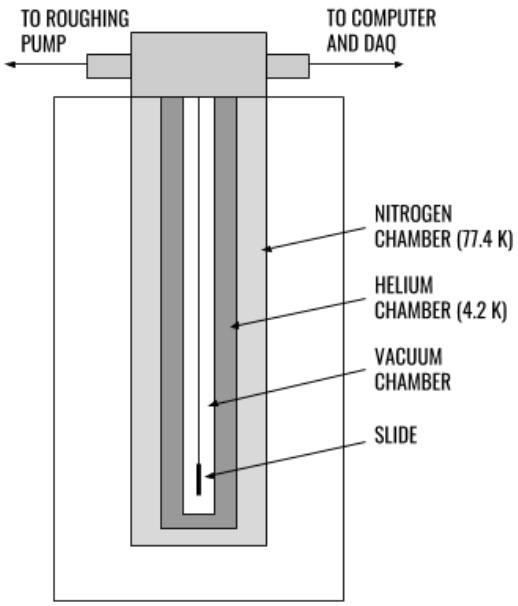

Figure II.2. A diagram of the cryostat. Temperatures indicated refer to the boiling point of the given liquid at atmospheric pressure.

III. DATA ANALYSIS

Before we present our results, we will explain the meticulous error analysis this data has undergone.

A. Error Analysis

1. *Sources of Error*

As mentioned, our independent variable in this experiment was the current we send through our junction. This resulted in a $V(I)$ curve where the voltage across our junction V_j was measured as a function of the current across our junction I_j. In practice, it is important to note that we were able to construct a current across our junction I_j with our internal resistor R_v. Namely, we divided our circuit driving voltage V_{tot} by our very large internal resistance $R_v \approx R_{tot}$, which was approximately our circuits total resistance, to find the total current going through our circuit $I_{tot} = I_j$, which was equal to the current going through our junction. However, for reasons detailed in V A, we found that the uncertainty in R_v was accounted for by our fitting of R_o in each regime; thus, we did not propagate this δR_v error.

We also realize that there was a finite precision uncertainty δV_{tot} of the voltages provided by our data acquisition system, which we calculated to be $\delta V_{\mathrm{tot}} = .005V$. However, for reasons elaborated upon in section V A, we did not propagate this error because the voltages we were supplying our circuit with were much larger than this fi-

nite precision.

So, for the sake of completeness, we have talked at length about potential sources of error that we choose to ignore in our error analysis. Now, let us finally get to a source of error that we actually decided to include!

Since we collected a large amount of samples at every time step, at every driving current I_j, we were able to calculate δV_j (error in measured voltages) from the standard deviation of our distribution of samples at every time step. We believe that this standard deviation of our samples at each time step included the effects of the finite resolution of each DAQ measurement, one that we also measured to be .005V. For this reason, we did not feel the need to separately include the finite resolution of each sample measurement in a calculation of the error bars of V_j.

Finally, we found a constant V_j offset in our data that we felt compelled to correct. The trials that we ran to determine the dependence, or lack thereof, of this offset on parameters such as gain, frequency filter settings, R_v setting, and more helped us decide how to address this systematic offset. After much testing, we found that this offset occurred in a portion of our circuit both inaccessible to us and before our amplification of the V_j signal. The trials through which we confirmed the constant nature of this offset are elaborated upon in V A.

In this way, we were able to calculate the vertical (δV_j) error bars of our $V(I)$ curve.

2. Error Propagation

The next step in our analysis involved taking our $V(I)$ curve and flipping both its points and the associated error bars to obtain a $I(V)$ curve.

We then aimed to propagate the δV_j (now horizontal error bars) in our error analysis calculations. We did this by propagating our horizontal error bar (δV_j) in our $I(V)$ curve into associated vertical (δI_j) error bars.

It is generally true that $\delta f(x) = \frac{\partial f(x)}{\partial x}\delta x$. We used this relation and the *approximately* linear resistor nature of our junctions in every regime (NIN, SIN, SIS) at large voltage ranges to simplify the $f(x)$ describing our $I(V)$ curve. This was a necessary step in propagating our horizontal error bars into something that could contribute towards our vertical error bars. Specifically, we assumed that:

$$I_j = \underbrace{\frac{1}{R_j}}_{m=\text{ slope}} V_j \tag{III.1}$$

This relation allowed us to find the effective junction resistance of our junctions by linearly fitting the data we collected. By calculating the line of best fit for our $I(V)$ curves in the NIN Regime we were able to find $R_o = \frac{1}{m}$. Similarly, an approximate calculation of $R_o \pm \delta R_o$ in the SIN and SIS regime using the tail ends of our data gave us an estimate useful for R_o useful in propagating our δV_j to δI_j. Again, we used this approximation to calculate the propagation of our horizontal error bars to vertical error bars, in the following way:

$$\delta I(V)_{\text{horizontal}} = \sqrt{\left(\frac{V_j}{R_j^2}\delta R_j\right)^2 + \left(\frac{1}{R_j}\delta V_j\right)^2} \tag{III.2}$$

B. Reduced χ^2

While we were able to account for statistical errors at each point of our measurement record by using vertical error bars (δI_j), there are systematic errors and fit parameters in our theory that we must optimize and account for to get the best possible theoretical fit curve to compare to our data. These fit parameters also contain useful information about the nature of the materials used in our experiment, as we will soon see.

1. Free Fit Parameters

Namely, these free fit parameters include $R_\parallel$, δ_{Pb}, δ_{Al}, T, and R_o. $R_\parallel$ is a parameter that arise from the presence of a large but finite resistance in parallel with our junction or a small by nonzero resistance in series with our junction, both of which can smear out our $I(V)$.

δ_{Pb} and δ_{Al} represent the superconducting energy band levels that open up between allowed electron states when Pb and Al become superconducting respectively.

T is the temperature of our junction and R_o is a temperature independent constant roughly related to the approximate linear resistance of our junction at any regime. In the NIN regime, R_o is exactly equal to R_j, which is the slope of the NIN $I(V)$ curve.

While we can calculate R_o for each junction through our experiments in the NIN regime, we must try to fit R, δ_{Pb}, δ_{Al}, and T to find the theoretical curves $I(V)$ closest to our experimental $I(V)$ curves in the SIN and SIS regimes respectively.

2. Reduced χ^2 Minimization

A common measure used to find fit parameters that minimize the deviation of experimental values from theoretical predictions is the reduced χ^2 metric. This metric can be roughly thought of as the distance between the experimental curve and the theoretical curve. Clearly, as we adjust the fit parameters that determine this theoretical curve, our reduced χ^2 measure will change to reflect the closeness or distance between the changing theoretical curve and static experimental curve. Thus, if we traverse a relevant parameter space and calculate this reduced χ^2 value for enough points on this space, we will be able to find the point in our parameter space that

minimizes our reduced χ^2 and gets our theoretical curve as close as possible to our experimental curve. Formally, our reduced χ^2 can be written as χ^2_ν and calculated as follows:

$$\chi^2_\nu = \frac{1}{\nu} \underbrace{\sum_{i=1}^{N} \frac{(y_i - f(x_i, \alpha))^2}{\sigma_i}}_{\chi^2} \tag{III.3}$$

where y_i are the N experimental data points, $f(x_i, \alpha)$ are the y values of our theoretical curve given parameters α, and σ_i is the uncertainty in y_i. In addition, $\nu = N - p$ is the number of data points N minus number of parameters p we are free to change. This ν reflects the true degrees of freedom our experimental graph may have. The greater the degrees of freedom, the larger the ν we have to divide our χ^2 by to get a true measure of how close our experimental curve is to our theoretical curve given some parameters α. In other words, we are more forgiving of larger χ^2 values if there are more degrees of freedom ν for our experimental curve to differ from our theoretical curve on.

In summary, we will explore a grid of parameter choices and choose the one that minimizes our χ^2_ν measure. This will leave us with the theoretical $I(V)$ curve closest to our experimental data; in turn, we will be able to find the best estimates of our fit parameters. The closer our χ^2_ν is to 1 the better. $\chi^2_\nu < 1$ implies over-fitting, and $\chi^2_\nu >> 1$ implies inaccuracy of our model.

3. Initial Parameter Estimation

There are four parameters for which we needed initial estimates to begin our χ^2 optimization. These free fit parameters are R_o, T, Δ_{Al}, and Δ_{Pb}. Note that after attempting to optimize over $R_\parallel$, a stray junction connection effect, we found that our χ^2_ν was monotonically smaller as we increased $R_\parallel$. This led us to believe that $R_\parallel$ was both unnecessary to fit and unnecessary to include in our calculations of the theoretical $I(V)$ curves in any regime.

R_o can be interpreted as the apparent resistance of the junction far from superconducting behavior. Thus, the slope of a linear fit in the region (d) of Fig. I.2 gives a good estimate for $R_o \approx R_{\text{linear fit}}$ [3]. Thus, for the χ^2 grid we varied R_o from $R_{\text{linear fit}} - 10\Omega$ to $R_{\text{linear fit}} + 10\Omega$ for the SIN optimization. We used the same approximation technique to find a R_o parameter range to vary R_o through for the SIS and NIN optimizations.

For the SIN case, we could estimate the temperature to be equal to the boiling point of liquid helium at 760 Torr, that is, 4.2 K. So, we gave T a range from 4.0 K to 4.4 K for our χ^2_ν grid. The SIS case, however, is more complicated because the boiling point of helium is decreased by the change in pressure. At the beginning of our SIS regime data collection the pressure was 1.684 Torr and had decreased to 1.164 Torr by the end. This corresponds to a boiling point of helium between 1.27 Torr and 1.39 Torr [4] [2]. Thus, for our χ^2 grid we varied temperature from 1.1 K to 1.4 K for the SIS optimization.

Estimates for the two superconducting gaps Δ_{Al} and Δ_{Pb} can adequately be obtained just by inspecting the data. We know that the the gap value is about equal to (e times) the voltage value at which current jumps from 0 to the finite value $R_o V$. In effect (when T is nonzero), this point is fairly ambiguous, but we felt confident in estimating Δ_{pb} to be – in the SIN regime – between 0.9 meV and 1.3 meV. In the SIS regime, we use the theory we detailed in to estimate Δ_{Pb} and Δ_{Al} to be around 1.3 meV and 0.05 meV, respectively. We ranged close to these estimated values.

4. Optimal Parameters with Uncertainty

To ascribe uncertainty to our best fit parameter estimates, we varied each parameter individually around its best fit value and calculated the adjoining new χ^2_ν value until this new value was at least double our minimum χ^2_ν value. In effect, we found a range around our best fit parameter values that reflected reasonable uncertainty in these parameter estimates.

5. Residuals

An analysis of the residuals from a χ^2_ν fit can help determine if the fit is actually correct. Since our residuals in the case of Junction 3 are almost identical to the residuals of our Junction 2 fit, we will only graph our Junction 2 residuals.

The residual for data point i is

$$\epsilon_i(x_i) = \frac{y_i - f(x_i, \alpha^*)}{\sigma_i} \tag{III.4}$$

where $f(x_i, \alpha^*)$ is the theoretical value at x_i as determined by the χ^2 minimization to get the best fit parameters α^*. These residuals add in quadrature to give

[3] In fact, since the theoretical $I(V)$ curve is an even function in every regime, we can fit perform a linear fit on the tail ends of our data, which essentially gives a line that the tails of the curve are approaching, the slope of which gives a good R_o estimate.

[4] The other method for measuring temperature uses the lock-in amplifier. After measuring an initial resistance R_1 and temperature T_1, and then decreasing the pressure until a resistance R_2, the final temperature T_2 is given by the relation $R_2/R_1 = \ln(T_1/T_2)$. This method gave a temperature of 1.16 K, which was lower than we expected.

the χ^2 value, and while minimizing this sum is important, it is also important that the residuals be roughly randomly distributed. A residual plot should be normally distributed around zero with standard deviation one. Fig. III.1 shows the residuals for the NIN fit; Fig. III.2 shows the residuals for the SIN fit; and Fig. III.3 shows the residuals for the SIS fit.

Generally, these plots look good enough for the fits to be trusted, but a couple features are of note. In Fig. III.1, the residuals have a smaller deviation around 0 than expected, indicating overestimated error. In Fig. III.2, the tails veer away from zero, which contributes significantly to the respective χ^2 value.

We can also see in III.3, that the data points right before and after the regions of predicted negative resistance (points near the mini voltage peaks) in our voltages produce the greatest residual values, which in turn contribute greatly to the minimum χ^2_ν value we can get for our SIS regime. While we removed data points in the region where our theoretical curve predicts negative resistance, we were hesitant to remove data points right before and after these regions of predicted negative resistance on our I(V) curves. We hesitated to do this because we believed that these data points were essential in finding our Δ_{Al} and Δ_{Pb} parameters and characteristic of the uniqueness of the SIS regime. The cost of this choice is evidently a larger χ^2_ν. We can also see that we have generally underestimated our error in the SIS case.

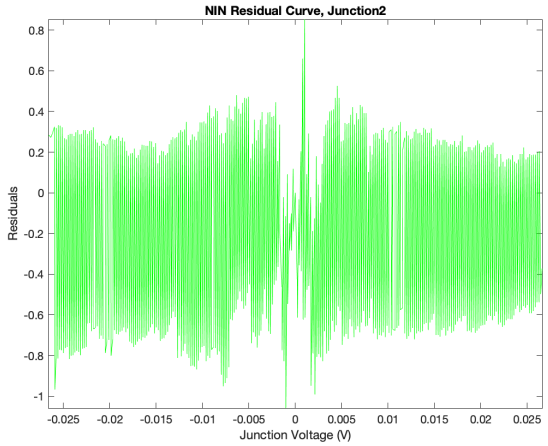

Figure III.1. A plot of the residuals for junction 2 in the NIN regime corresponding to the Fig. III.4 fitted curve. The random distribution indicates a good fit. However, the consistent magnitude around .4, as opposed to around 1 indicates that we overestimated the error in the respective data.

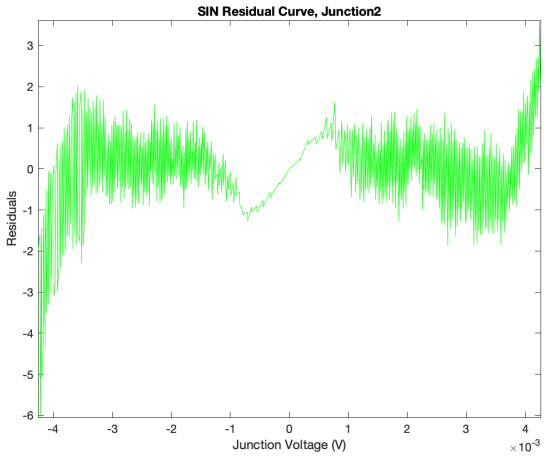

Figure III.2. A plot of the residuals for junction 2 in the SIN regime corresponding to the Fig. III.5 fitted curve. The random distribution between $-3\,\mathrm{mV}$ and $3\,\mathrm{mV}$ about equal in magnitude to 1 is an indication of a good fit. However, the behavior in the tails does generate some concern.

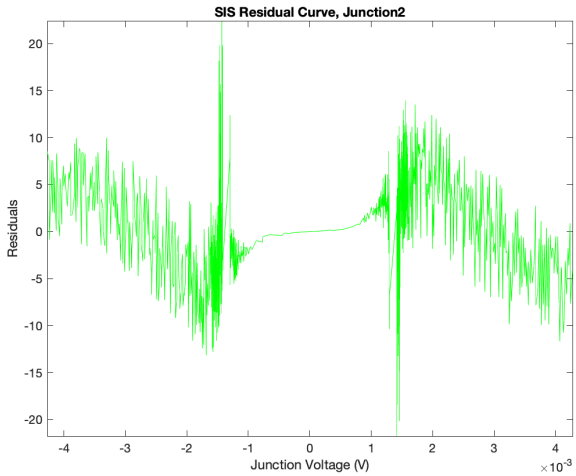

Figure III.3. A plot of the residuals for junction 2 in the SIS regime corresponding to the Fig. III.6 fitted curve. As represented in the relatively large magnitude residuals, we generally underestimated the error on our SIS data. We also see spikes before and after regions of predicted negative resistance, which are an unavoidable artifact of the sharpness of our theoretical curve and the finite step size of our data. Thus, the spike in residuals at $\pm 1.5\,\mathrm{V}$ is to be expected.

C. Results

After running the χ^2_ν minimization for each regime as described, we were left with the following fit parameters that minimized our χ^2_ν and best theoretical fits.

While we have only displayed the best fit theoretical curve for Junction 2, we have calculated this curve and listed the associated best fit parameters for every working junction. We have found the best fit curves to look very

similar to the case of Junction 2 for Junction 3 in all regimes, so we will only display our graphs for Junction 2.

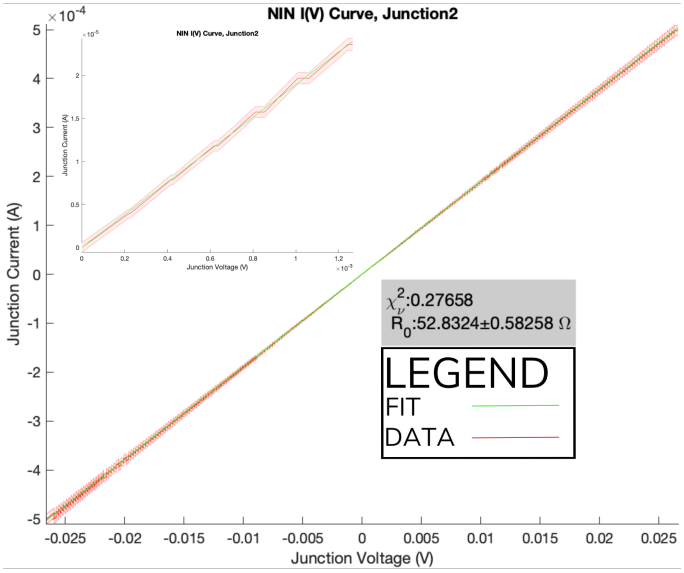

Figure III.4. NIN Junction 2 I(V) Curve

Junction	1	2	3	Avg
χ_ν^2	.328	.277	.213	0.273
$R_o(\Omega)$	$54.0 \pm .7$	$52.8 \pm .6$	$57.5 \pm .6$	$54.8 \pm .6$

Table III.1. Best Fit Parameter Estimates for NIN Regime

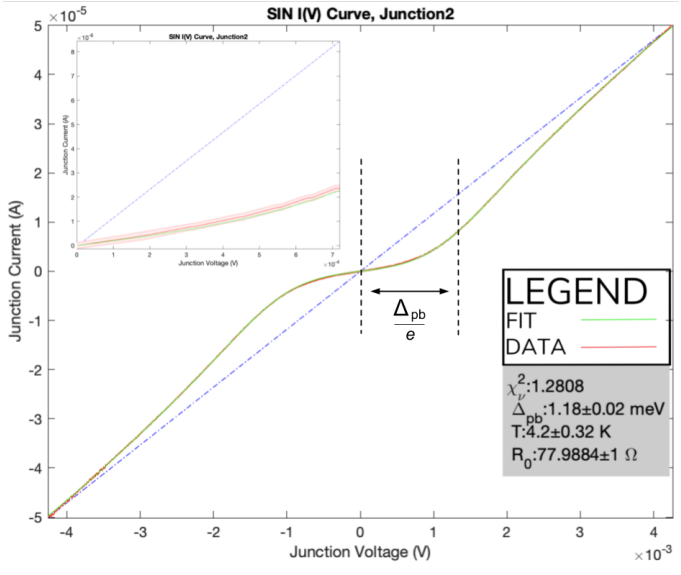

Figure III.5. SIN Junction 2 I(V) Curve

Junction	2	3	Avg
χ_ν^2	1.28	2.74	2.01
$R_o(\Omega)$	78 ± 1	84 ± 1	81 ± 1
T(K)	$4.2 \pm .3$	$4.0 \pm .3$	$4.1 \pm .3$
Δ_{Pb}(meV)	$1.18 \pm .02$	$1.18 \pm .04$	$1.18 \pm .02$

Table III.2. Best Fit Parameter Estimates for SIN Regime

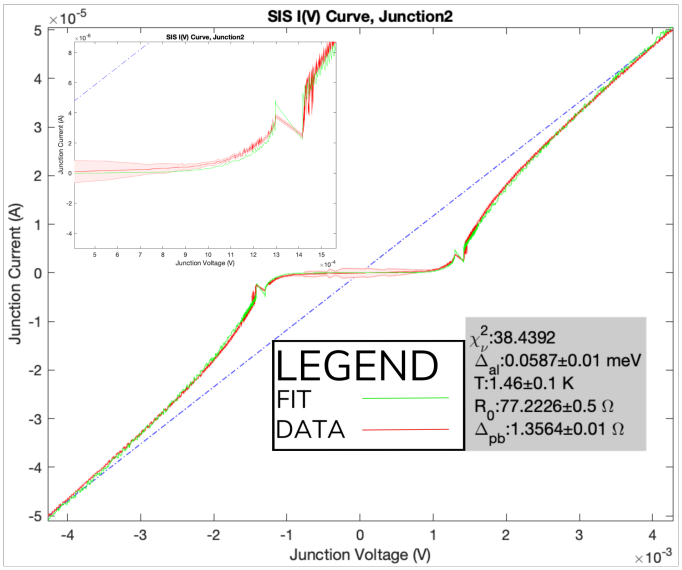

Figure III.6. SIS Junction 2 I(V) Curve

D. Interpretations

1. *NIN*

As shown in Figure III.4 and Table III.1, we were able to verify the linear relationship between junction current and junction voltage as predicted by Eq I.1. We realize that we may have overestimated our error in the NIN case, leading to a $\chi_\nu^2 < 1$ and a residuals curve normally distributed around zero but with mean less than one. Perhaps, some of the error we propagated was unnecessary, such as the driving voltage and R_v uncertainty. Regardless, our data followed a linear trend as expected.

2. *SIN*

Our excellent minimum χ_ν^2 values for our SIN best theoretical $I(V)$ curve fits as shown in Table III.3 and Figure III.5, along with appropriate residual graphs as shown in Figure III.1 strongly motivate our confidence in our best fit parameter estimates. Notably, our residuals seem to deviate from their otherwise standard normal distributed behaviour at the tail ends of our Junction Voltage values. Perhaps it is this deviation that raised our χ_ν^2 slightly above 1. Still, we can remain confident in our estimations of Δ_{pb} as they are unaffected by this slight deviation in

Junction	2
χ^2_ν	38.44
$R_o(\Omega)$	$77.2 \pm .5$
T(K)	$1.46 \pm .1$
Δ_{Pb}(meV)	$1.36 \pm .01$
Δ_{Al}(meV)	$.0587 \pm .01$

Table III.3. Best Fit Parameter Estimates for SIS Regime

the asympotitic nature of the SIN I(V) curve. The Δ_{pb} estimates are unaffected because their influence on the shape of our $I(V)$ curve is strongest near 0 and weakest near the tail ends of our $I(V)$ curve. This discrepancy in the residuals of our SIN curve would instead most likely affect our R_o estimate, which is more influential in the asymptotic nature of our $I(V)$ curve.

3. SIS

While our χ^2_ν is not as low as in the SIN case, our SIS residual curve in Figure III.2 shows us possible sources of this large χ^2_ν as detailed in III B 5. We also see from Figure III.6 that our theoretical curve nicely aligns with our measured data. These factors lead us to believe that our Δ_{Pb} and Δ_{Al} estimates are reasonable. When analyzing our junction 3 SIS data, we discovered that the relevant forward and backwards sweeps did not align at large voltages. This and unreasonably large χ^2_ν values for fits on junction 3 SIS data led us to believe that there was a systematic error in one of the sweep directions on junction 3, which is why we only calculated fit parameters for junction 2 for the SIS regime.

IV. CONCLUSION

Having reduced our χ^2 to 1.28 for the SIN regime and to 38.44 for the SIS regime, we predict the superconducting gap of lead to be 1.18 ± 0.02 meV at 4.2K and $1.36 \pm .01$meV at around 1.46K, and the superconducting gap of aluminum to be $.06 \pm 0.01$ meV at around 1.46K. Our low χ^2 value for the former regime makes us 66% confident in our Δ_{Pb} result. The larger χ^2 value for the latter regime makes us less confident in our Δ_{Al} result, as reflected in the greater percentage uncertainty.

Given the largely pedagogical motivation for this experiment, there are a couple instances where more care could have been taken to decrease error in our results. We discuss these cases in the appendix, and reason why we felt we could ignore them. With our time constraints, though, we feel we have struck a fair balance between efficiency and scientific rigor.

V. APPENDIX

A. Nuances of Error Analysis

One issue we encountered at the beginning of our experiment with our data collection equipment was the presence of an offset in voltage measured. When using the test resistor, we consistently observed that our $I(V)$ curve was not centered at $(0, 0)$. We considered that this could possibly be error induced at some point in the measurement circuit, and thus dependent on one of the settings (whether that be the internal resistor, gain, sample rate, or direction of sweep). First, we found that it was not dependent on the direction of sweep, the sample rate, the internal resistor, or the measurement device itself. Yet, when we tested for dependence on gain, we found that the offset did change magnitude, meaning that the offset was occurring before the amplifier in the circuit. We resolved to subtract a constant offset from our data, and measured the appropriate value to be 1.67 mV with an associated uncertainty of 0.01 mV, to be added in quadrature to the error in each data point.

There were also several theoretical sources of error that we decided to ignore for various reasons.

The first was the precision of the output voltage of the DAQ (the voltage supplied to the circuit from the computer). We connected the output to the amplifier, and the amplifier to the DAQ input. Then, we stepped through voltages with the gain set to 200 and the voltages on the order of 10^{-2}. We found that the resolution of the DAQ output was 0.005 V. This means that a voltage cannot be supplied if it is not a multiple of 0.005 V. We thought this was a source of error, but realized that since the magnitudes of the voltages we were concerned with in the trials was significantly greater than this resolution. Thus, the device would have no issue supplying the voltage it was set to supply.

Using a similar technique, we found the same 0.005 V resolution in the measurement of voltage into the DAQ. However, the use of the amplifier ensures that the values we are trying to measure are significantly larger than the resolution of the device. Further, the 0.005 V precision is significantly smaller than the standard deviation of the measurements, meaning that the the potential error induced by this precision is already accounted for in the standard deviation of our data.

Another potential source of error is uncertainty in the resistance of the internal resistor. Yet, the internal resistor R_v is correlated to the fit parameter R_o (the slope of the $I(V)$ curve in the linear areas of each regime). Since this R_o is varied when optimizing χ^2, any uncertainty in R_v is accounted for.

The equation for the reduced chi-square is

$$\chi_{\nu^2} = \frac{1}{(f_f/f_s)N - p}\chi^2 \tag{V.1}$$

where f_f is the frequency of the filter and f_s is the frequency of the data sampling. In cases where $f_f < f_s$,

the denominator of Eq. V.1 is less than one, so chi-square increases. This makes sense because if $f_f < f_s$, the filter will make successive data points dependent. In isolation, this leads to a better fit, and a lower chi-square than would otherwise be achieved if the points were independent. However, we had $f_f > f_s$, meaning that the filter was not inducing any correlation between the data points. It does not make sense to multiply N by a factor greater than 1, because this would imply that the number of independent data points is actually greater than the number of data points. Thus, since N accurately represented the number of independent data points we had, we disregarded the (f_f/f_s) factor in Eq. V.1. [5]

B. Choosing our slide

In choosing our slide, we made voltage measurements of a significant number of the paths between contacts on each slide. Comparing measurements of equivalent paths between different slides gave us an idea of a ballpark range for what a good slide would look like. There was one slide that consistently gave different measurements than the rest, so we disregarded that one. Between the remaining five, all seemed like adequate candidates. We ended up choosing slide two because the resistance of the lead deposit was the most constant through its length. The resistance of the longest path was $141\,\Omega$. We were able to deduce that the resistances of the middle two sections were $44\,\Omega$ and $43.8\,\Omega$, and the resistances of the outer two sections were $27.7\,\Omega$ and $25.5\,\Omega$. The lengths of the sections compared here are equal, so the closeness of the measurements indicates a constant resistance. After choosing the slide we made more accurate voltage measurements using the apparatus, as discussed previously.

[1] Brubaker, B. (2016), "Phys 382 Superconducting Tunnel Junction Lab," .
[2] Keith, C. (2001), "Helium Vapor Pressure versus Temperature," .
[3] Schmitt, R. W. (1961), "The Discovery of Electron Tunneling into Superconductors," *Physics Today*, 14, 38.

[5] Professor Lamoreaux guided us through this reasoning.